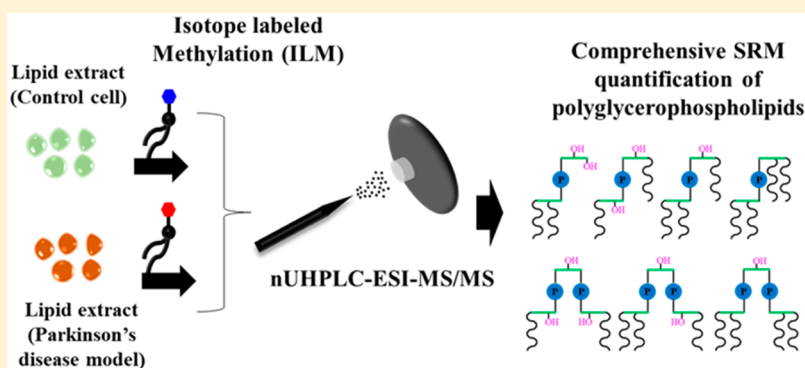


Simultaneous Relative Quantification of Various Polyglycerophospholipids with Isotope-Labeled Methylation by Nanoflow Ultrahigh Performance Liquid Chromatography-Tandem Mass Spectrometry

Jong Cheol Lee, Joon Seon Yang, and Myeong Hee Moon*

Department of Chemistry, Yonsei University, 50 Yonsei-ro, Seodaemun-gu, Seoul 03722, Korea

 Supporting Information

ABSTRACT: Herein, we introduce a comprehensive analytical method for the separation and relative quantification of polyglycerophospholipids (PGPLs), including phosphatidylglycerol (PG), bis(monoacylglycero)phosphate (BMP), bis(diacylglycero)phosphate (BDP), Hemi BDP, cardiolipin (CL), monolysocardiolipin (MLCL), and dilyocardiolipin (DLCL), using isotope-labeled methylation (ILM) with nanoflow ultrahigh performance liquid chromatography-electrospray ionization-tandem mass spectrometry (nUHPLC-ESI-MS/MS). Abnormal levels of BMP and CL have been associated with the pathology of lysosomal storage and neurodegenerative diseases. Thus, simultaneous analysis of all PGPLs is important to understand the mechanisms and pathologies of such diseases. In this study, improved separation and MS detection of PGPLs, including their regioisomers, was achieved by the methylation of PGPL. ILM-based relative quantification was applied to lipid extracts from a dopaminergic cell line (SH-SY5Y) treated with drugs commonly used for Parkinson's disease (PD), resulting in the identification of 229 unique PGPLs, including 121 CLs, 71 MLCLs, and 16 Hemi BDP species. The drug treatment induced significant increases in the amount of CLs containing polyunsaturated fatty acyl chains, including 20:4 and 22:6, as well as decreased levels of BMP, Hemi BDP, and BDP species, demonstrating the feasibility of using ILM for the comprehensive and high-speed relative quantification of PGPLs.

Polyglycerophospholipids (PGPLs) are phospholipids (PLs) that contain two or three glycerol molecules joined by a phosphodiester linkage. Members of this group include phosphatidylglycerol (PG), bis(monoacylglycero)phosphate (BMP), bis(diacylglycero)phosphate (BDP), Hemi BDP, diposphatidylglycerol or cardiolipin (CL), monolysocardiolipin (MLCL), and dilyocardiolipin (DLCL).¹ PG, BMP, Hemi BDP, and BDP contain two glycerols whereas DLCL, MLCL, and CL contain three glycerols. PGPLs exist exclusively in specific subcellular organelles such as mitochondria and lysosomes and perform characteristic roles. BMP, a structural isomer of PG, is enriched in the late endosome (~15%) and is involved in the transportation of proteins and cholesterol to the lysosome. The relative BMP content is approximately 1% when considering all PLs present in vivo.^{2,3} BMP accumulates in lysosomal storage diseases such as Niemann-Pick type C

disease, Gaucher disease, and drug-induced phospholipidosis.^{4–6} CL, a unique PL that is localized in the inner mitochondrial membrane (enriched up to 20%), is involved in maintaining membrane fluidity, producing ATP, and controlling the activity of cytochrome C oxidase during apoptosis.^{7,8} CL has been implicated in various diseases that feature increased levels of oxidative stress, including diabetes, heart failure, aging, neurodegenerative diseases (Alzheimer's and Parkinson's), and genetic disorders (Barth syndrome and Tangier disease).^{9–12} Because of the increased concentration of BMPs and CLs in several diseases, the potential use of PGPLs as biomarkers is more promising than for other PLs.

Received: February 12, 2019

Accepted: April 22, 2019

Published: April 22, 2019

PGPLs are formed from a common precursor (PG) and are significantly affected by each other's presence and relative quantity. BMP can undergo acylation to produce Hemi BDP or BDP, and CL can be deacylated to form MLCL or DLCL.^{13–16} Thus, simultaneous analysis of PGPLs is important to understand their pathological roles in several diseases and associated mechanisms. However, PGPL analysis is often limited due to the complexity of their molecular structures and difficulty in resolving isomeric structures with current analytical methods. Studies have been performed to characterize the molecular structures of MLCLs and DLCLs from cells by off-line combination of two-dimensional high performance thin-layer chromatography (2D-HPTLC) and electrospray ionization mass spectrometry (ESI-MS). MLCLs from fibroblast cells as a marker for Barth Syndrome have been analyzed using high performance liquid chromatography (HPLC)-ESI-MS.^{17,18} The molecular structures of a few CLs have been determined from mouse heart and liver extracts using HPLC-ESI-MS/MS and from rat mitochondria via LC coupled with high resolution MS (HR-MS) with high-energy collisional dissociation (HCD).^{19,20} PG and BMP species have been characterized from breast cancer cells, as well as mouse heart and liver using hydrophilic interaction chromatography-tandem MS (HILIC-MS/MS)^{21,22} and shotgun analysis using only ESI-MS/MS without chromatographic separation.²³ However, these methods have not been thoroughly optimized for the simultaneous qualitative and quantitative analysis of all PGPL species.

Herein, we introduce the isotope-labeled methylation (ILM) method via ultrahigh performance liquid chromatography-electrospray ionization-tandem mass spectrometry (nUHPLC-ESI-MS/MS) for comprehensive separation and relative quantification of all PGPLs, including PG, BMP, Hemi BDP, BDP, CL, MLCL, and DLCL as well as their regioisomers. Methylation of PL was easily achieved at the PL phosphate group using trimethylsilyldiazomethane (TMSD) and methylated PLs were analyzed by ESI-MS alone and by supercritical fluid chromatography or LC coupled to ESI-MS.^{24–26} The methylation resulted in an increased hydrophobicity of the PLs, which enhances their separation in reversed phase nUHPLC and ionization efficiency for ESI-MS. These effects improved the sensitivity of MS detection. The ILM method utilizes H-labeled ($-\text{CH}_3$) and D-labeled (CHD_2) methylation for direct quantitative analysis of the two sets of samples without the need for internal standards.²⁷ The incorporation of ILM with nUHPLC-ESI-MS/MS in the earlier study resulted in a significant improvement in the identification of anionic lipids such as CL (43 CL species in total), which are often difficult to analyze using LC-MS. Since neurodegenerative disorders such as Parkinson's and Alzheimer's disease are closely associated with mitochondrial dysfunction and oxidative stress,^{28–30} a comprehensive analysis of CLs and BMPs including the entire range of PGPLs must be developed. This study evaluated the efficiency of PGPL methylation for differentiating various regioisomers by nUHPLC-ESI-MS/MS and demonstrated application of ILM to the neuroblastoma SH-SY5Y cell, a model cell line for the Parkinson's disease research, for the high-throughput and relative quantification of PGPLs and their isomers. The neuroblastoma cells were treated with the three most commonly used drugs (6-OHDA, MPP⁺, and rotenone) to mimic the Parkinson's disease model,³¹ and the lipid extracts of the drug-treated cells were analyzed along with a control via ILM-based quantification.

EXPERIMENTAL SECTION

Materials and Reagents. The PGPLs standards were purchased from Avanti Polar Lipids Inc. (Alabaster, AL, USA): PG 14:0/14:0, PG 18:1/18:1, BMP 14:0_14:0, BMP 18:1_18:1, Hemi BDP 14:0_14:0_14:0, Hemi BDP 18:1_18:1_18:1, BDP 18:1/18:1/18:1/18:1, DLCL 18:2_18:2 (bovine heart extract), MLCL 18:2_18:2_18:2 (bovine heart extract), CL 14:0/14:0/14:0/14:0, and CL 18:1/18:1/18:1/18:1. HPLC grade solvents were purchased from Avantor Performance Materials (Center Valley, PA, USA): H₂O, CH₃CN, CH₃OH, isopropanol (IPA), and methyl-*tert*-butyl ether (MTBE). Ionization modifiers (NH₄HCO₂, NH₄OH, and NH₄CH₃CO₂), CHCl₃, CD₃OD, HCl solution, trypan blue solution, 6-hydroxydopamine hydrobromide (6-OHDA), MPP⁺ iodide, and rotenone were purchased from Sigma-Aldrich (St. Louis, MO, USA). Deuterated water (D₂O), deuterium chloride (DCl, 20% (w/w) in D₂O), and TMSD (2 M in hexane) were purchased from Thermo Fisher Scientific (Waltham, MA, USA). Glacial acetic acid was purchased from Duksan Pure Chemicals Co., Ltd. (Ansan, Korea). Fused silica capillary tubes with inner diameters of 20, 50, and 100 μm , all with the same outer diameter of 360 μm , were purchased from Polymicro Technology, LLC (Phoenix, AZ, USA). The packing material used for the RPLC columns was ethylene bridged hybrid (BEH) C18 particles (1.7 μm and 130 Å) unpacked from an ACQUITY UPLC BEH C18 column (2.1 mm \times 100 mm) from Waters (Milford, MA, USA). Watchers ODS-P C18 particles (3 μm and 100 Å) from Isu Industry Corp. (Seoul, Korea) were used to fabricate a self-assembled frit of a pulled-tip analytical column prior to packing the 1.7 μm C18 particles.

Cell Culture, Drug Treatment, and Viability Tests. Human dopaminergic SH-SY5Y cells were obtained from Korean Cell Line Bank (Seoul, Korea). The cells were cultured in a 100 mm Petri dish in Dulbecco's Modified Eagle's Medium (DMEM) from Invitrogen (Carlsbad, CA, USA) with 10% heat inactivated fetal bovine serum (FBS) and 1% penicillin/streptomycin in an incubator at 37 °C under a humidified atmosphere with 5% CO₂ for 48–72 h. When the cells reached >90% confluency, they were detached by adding 0.25% trypsin-EDTA.

The same amount of cells (approximately 6.0×10^6 cells) were seeded in each of the four Petri dish: one for the control and the other three for drug treatments (100 μM 6-OHDA, 5000 μM MPP⁺, and 5 nM rotenone for 24 h in order to induce 50% cell death).³² After drug treatment, the cells were washed with PBS solution and centrifuged (2000g for 3 min at 4 °C). The cell pellets were subsequently used for lipid extraction. For the cell viability test, the trypan blue exclusion assay was applied. The cell suspension was mixed with an equivalent volume of 0.4% trypan blue solution for 1 min, and the noncolored viable cells were counted using a hemocytometer.

Lipid Extraction. The cell pellets were dried under nitrogen using an Evatros Mini evaporator from Goojung Engineering (Seoul, Korea) before lipid extraction, because water in the cell pellet competes with D₂O to affect the degree of D-methylation. The dried cell pellets were suspended in 170 μL of H₂O and homogenized using a tip sonicator for 2 min followed by addition of 80 μL of HCl for a final concentration of 2.05 M. Lipid extraction followed the previous study using methanol and MTBE.³³ To the mixture, 300 μL of CH₃OH

and 1.0 mL of MTBE were added. The mixture was then vortexed for 1 h and centrifuged at 1000g for 5 min. The upper organic layer was transferred to a new vial, and the remaining lower layer was extracted again by adding 400 μL of an upper organic layer of MTBE/ $\text{CH}_3\text{OH}/\text{H}_2\text{O}$ (10:3:2.5, v/v/v). After 10 min of vortexing, the organic layer was retrieved and combined with the previously collected organic layer. The resulting mixture was washed with 500 μL of the lower aqueous layer of the previously used solvent mixture (MTBE/ $\text{CH}_3\text{OH}/\text{H}_2\text{O}$), vortexed for 10 min, and centrifuged at 3000g for 5 min. The final organic layer containing the extracted lipids was used for lipid methylation.

Isotope-Labeled Methylation (ILM). PGPL methylation was achieved following the procedures described in detail in a previous report.²⁷ Briefly, the organic layer of the cellular lipid extracts or PGPL standard mixture was added to 100 μL of CH_3OH and 50 μL of TMSD (2 M in hexane) and incubated for 10 min at room temperature. To remove excess TMSD, 6 μL of glacial acetic acid was added. The mixture was then washed by adding 500 μL of the lower aqueous layer of the solvent mixture (MTBE/ $\text{CH}_3\text{OH}/\text{H}_2\text{O}$), followed by 10 min of vortexing and subsequent centrifugation at 3000g for 5 min. The methylated lipids were dried under nitrogen and dissolved in $\text{CH}_3\text{OH}/\text{CHCl}_3$ (9/1, v/v) for nUHPLC-ESI-MS/MS analysis. ILM for relative quantitation of the lipids was performed by replacing CH_3OH , H_2O , and HCl with CD_3OD , D_2O , and DCl, respectively.

nUHPLC-ESI-MSⁿ Analysis. Identification and quantification of lipids were achieved by using the two nUHPLC-ESI-MS/MS systems; a Dionex Ultimate 3000 RSLCnano System with LTQ Velos ion trap mass spectrometer from Thermo Scientific (San Jose, CA, USA) for the global identification of lipids and a nanoACQUITY UPLC instrument from Waters (Milford, MA, USA) coupled with a TSQ Vantage triple-stage quadrupole mass spectrometer from Thermo Scientific for targeted selected reaction monitoring (SRM) quantification. Capillary columns were prepared in the laboratory with a silica capillary (100 μm inner diameter) by pulling one end of tube with a flame to form a sharp tip as a self-emitter for ESI. The end (5 mm in length) of the pulled-tip column was filled with Watchers ODS-P C18 particles (3 μm) to create a self-assembled frit, and the remaining 8 cm was packed with BEH C18 particles (1.7 μm) under nitrogen gas at 1000 psi.³⁴ The column connection with UHPLC was identical to that reported elsewhere.²⁷ The mobile phase solutions were $\text{H}_2\text{O}/\text{CH}_3\text{CN}$ (9:1, v/v) for A and $\text{CH}_3\text{OH}/\text{CH}_3\text{CN}/\text{IPA}$ (2:2:6, v/v/v) for B. As ionization modifiers of the intact PGPLs, 0.05% ammonium hydroxide (AH) was added to both mobile phase solutions for analysis in negative ion mode. For separation of the methylated PGPLs, 5 mM ammonium formate (AF) was used for analysis in positive ion mode.

For lipid identification, approximately 10 μg of methylated lipid extract or a mixture of PGPL standards (1 pmol each) was injected into the analytical column with mobile phase A at 750 nL/min for 10 min. Subsequently, the UHPLC pump flow rate was increased to 10 $\mu\text{L}/\text{min}$ with the split valve on, resulting in 300 nL/min of column effluent. Gradient elution was initiated by increasing mobile phase B to 60% for 0.1 min, then to 90% for 5 min, which was maintained for another 5 min, and further to 99% for 15 min and maintained for 8 min. The column was then re-equilibrated by decreasing mobile phase B to 1% for 7 min for the next run. The ESI voltage was set to 3.0 kV, and m/z range of the full MS scan was 400–

1600. Data-dependent CID analysis was operated at a 40% normalized collision energy. The lipid molecular structures were identified by Lipilot software based on the CID product ion spectra, which was developed in house³⁵ and manually confirmed.

Quantification of the H- and D-methylated PGPLs was performed using the SRM method. Lipid extracts from the control cells were H-methylated, and those from the drug treated cells were D-methylated. The same analytical column used for lipid identification was again used but with different gradient elution conditions to increase the rate of quantification. The 1:1 (v/v) mixture of H- and D-methylated lipid extract samples was vortexed for a while and injected with mobile phase A at 850 nL/min for 10 min. After sample loading, the pump flow rate was raised to 13 $\mu\text{L}/\text{min}$ and the final column flow rate was adjusted to 300 nL/min using a split valve. The gradient elution was initiated by changing mobile phase B to 60% for 0.1 min; 90% for 5 min; 95% for 3 min; 100% for 7 min, maintained for 10 min. Thereafter, 0% B was pumped 5 min to re-equilibrate the column. SRM quantification of the PGPLs was achieved in positive ion mode at an ESI voltage of 3.0 kV, scan width of m/z 1.0, and scan time of 0.001 s. The SRM table was established for each lipid species assigned with a precursor ion, a product ion as a quantifier ion, and a specific CID energy within a programmed time interval ($t_r \pm 1$ min) for detection.³⁶ The CID energies specific for each lipid class preliminarily optimized are listed in Table S1.

RESULTS AND DISCUSSION

nUHPLC-ESI-MS/MS Analysis of the Methylated PGPLs. Methylation enhances PGPL analysis by increasing the hydrophobicity of the anionic lipids, resulting in increased retention time and improved MS detection. Figure 1 compares the extracted ion chromatograms of a mixture of 11 PGPL

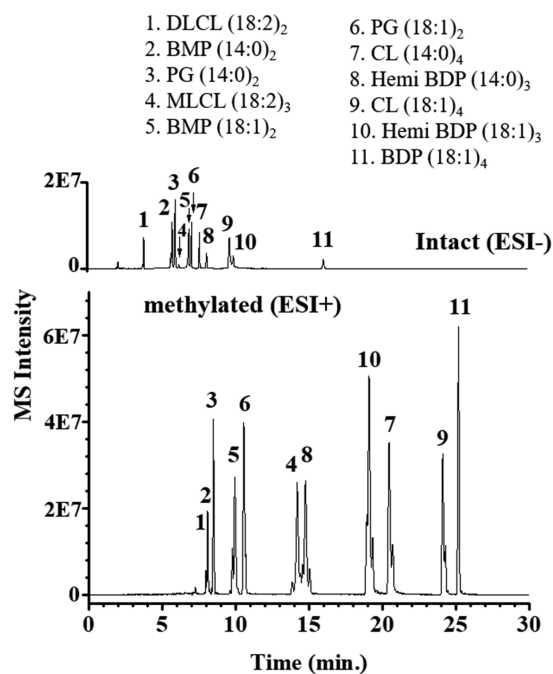


Figure 1. Base peak chromatograms of the standard PGPL species before (intact) and after methylation obtained by nUHPLC-ESI-MS/MS.

standards before (top) and after (bottom) methylation obtained by nUHPLC-ESI-MS. The intact PGPLs species were detected in negative ion mode whereas the methylated PGPLs were run in positive ion mode and showed significant increases in peak intensities and retention times depending on methylation extent. Because CLs including MLCL and DLCL contain two phosphate groups for two methylations while PG-based PGPLs including BMP, Hemi BDP, and BDP contain only one phosphate, the retention time increases of the methylated CL series (peaks 1, 4, 7, and 9) were larger than those of the PG series in the reversed phase column. Mass spectra of the intact and methylated species were obtained under negative and positive ion mode, respectively, preventing a direct comparison of peak intensity values. Therefore, peak intensities of the methylated PGPL species in Figure 1 were compared using the signal-to-noise ratio (S/N) of each peak to those of the intact species in Table 1. The S/N was calculated

Table 1. Signal-to-Noise (S/N) Ratio of the Intact (I) and Methylated (M) PGPLs Including Regioisomers (R) by nUHPLC-ESI-MS/MS from Figure 1

PGPL species	R	S/N		
		I	M	M/I
1. DLCL (18:2) ₂	(1)	2	349	146.5
	(2)	33	451	13.7
	(3)	261	1601	6.1
	(4)	N.D.	83	NEW
2. BMP (14:0) ₂	(1)	16	13	0.8
	(2)	128	129	1.0
	(3)	389	444	1.1
3. PG (14:0) ₂		577	934	1.6
4. MLCL (18:2) ₃	(1)	N.D.	67	NEW
	(2)	31	598	19.3
	(3)	329	626	1.9
5. BMP (18:1) ₂	(1)	35	24	0.7
	(2)	329	248	0.8
	(3)	329	626	1.9
6. PG (18:1) ₂		386	918	2.4
7. CL (14:0) ₄		305	807	2.7
8. Hemi BDP (14:0) ₃	(1)	N.D.	161	NEW
	(2)	125	609	4.9
9. CL (18:1) ₄	(1)	255	750	2.9
	(2)	104	1164	11.2
10. Hemi BDP (18:1) ₃	(1)	N.D.	428	NEW
	(2)	104	1164	11.2
11. BDP (18:1) ₄		80	1426	17.7

for each regioisomer, and the structural determination (see Figure S1) by MS/MS will be explained later. The S/N ratios of the methylated PGPL species increased for most PGPL species (2–146-fold). In addition, four regioisomers were newly identified after methylation: DLCL (18:2)₂ (4), MLCL (18:2)₃ (1), Hemi BDP (14:0)₃ (1), and Hemi BDP (18:1)₃. However, decreased ionization efficiency for the relatively low abundance BMP regioisomers was also observed. To thoroughly validate the enhancement of sensitivity, the limit of detection (LOD, 3s/m, s = standard deviation of the y-intercept, m = slope of calibration curve) and limit of quantitation (LOQ, 10s/m) were calculated from the calibration curve based on the peak area ratio of each PGPL standard obtained by the SRM method. LOD values (fmol unit) were found to range from 20.5 for Hemi BDP (14:0)₃ to 321.3 for BDP (18:1)₄ in their intact conditions and from 2.92 for MLCL (18:2)₃ to 21.38 for PG (14:0)₂ after methylation as

listed in Table S2, supporting that the sensitivity for PGPL standards can be increased about 10-fold after methylation.

Regioisomers of the PGPLs were differentiated by retention times and MS/MS spectra obtained from the nUHPLC-ESI-MS/MS analysis upon methylation. For instance, the extracted ion chromatogram of peak no. 4 in Figure 1 ($[M_H + NH_4]^+$, m/z 1232.9, subscript H indicating H-methylation) is shown in Figure 2 as an example of the separation of the two

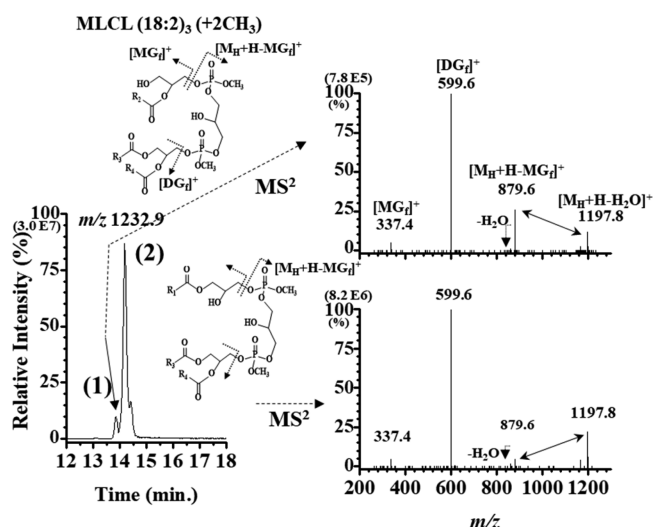


Figure 2. Extracted ion chromatogram (EIC) of m/z 1232.9 ($[M_H + NH_4]^+$) from the two regioisomers of the methylated MLCL (18:2)₃ shown with molecular structures and associated MS/MS spectra of peaks (1) and (2). See Figure S1 for the proposed CID mechanisms of the regioisomers.

regioisomers of MLCL 18:2_18:2_18:2 or simply MLCL (18:2)₃. The isomers can be distinguished by the relative intensities of the two characteristic fragment ions in their respective MS/MS spectra. Peaks (1) and (2) in Figure 2 originated from molecular structures with single acyl chain located at the sn-2 and sn-1 positions of the glycerol backbone, respectively. However, the dissociation of the bond between glycerol and phosphate group of a molecular structure (1) containing the sn-2 acyl chain (see molecular structure in the chromatogram) occurs preferentially over the cleavage from the relatively extended structure (2) with less steric hindrance. Therefore, formation of the remaining fragment ion $[M_H + H - MG_f]^+$ (m/z 879.6; MG_f denotes the monoacylglycerol fragment) from (1) is preferred over that from (2). The possible fragmentation pathways are described in detail in Figure S2. Because of the difference in the regioisomeric structures of MLCL (18:2)₃, the relative peak intensities of $[M_H + H - MG_f]^+$ ($25.3 \pm 0.6\%$ for (1) and $4.7 \pm 0.3\%$ for (2)) and $[M_H + H - H_2O]^+$ ($11.9 \pm 0.8\%$ for (1) and $23.3 \pm 1.0\%$ for (2)) were reversed in the isomeric structure (2) where the single acyl chain is located at the sn-1 position. This leads to a stronger interaction with the RP stationary phase, resulting in longer retention times. The small shoulder at the end of peak (2) is presumed to be an isomeric structure with a methylation on the hydroxide in the central glycerol backbone between the two phosphate groups due to a mis-methylation. However, the structure cannot be determined solely from the CID spectra because the two $[M_H + H - MG_f]^+$ ions from different structures have the same m/z .

The methylated BMP regioisomers and PG moieties containing the same acyl chains were clearly distinguished by nUHPLC and their CID spectra. BMP (18:1)₂ and PG (18:1)₂ (peaks 5 and 6, respectively, in Figure 1) share the same mass, but the extracted ion chromatogram of m/z 806.7 ($[M_H + NH_4]^+$) shows a clear separation of the three BMP regioisomers (1)–(3) and PG (Figure 3). The MS/MS

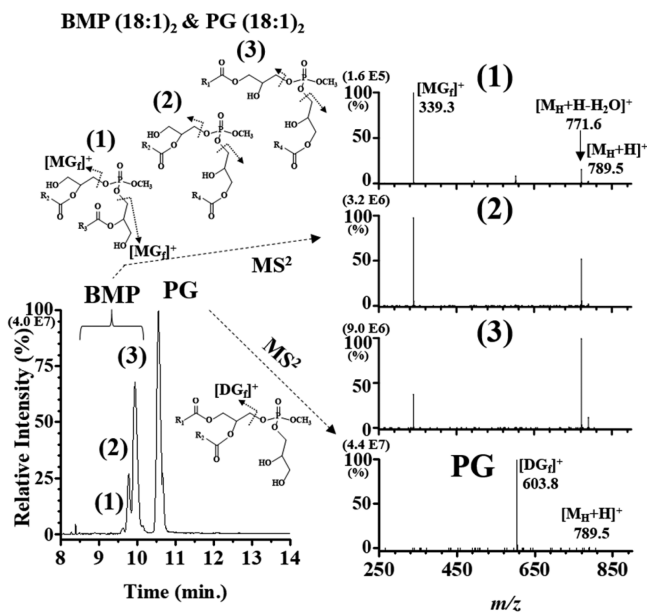


Figure 3. Extracted ion chromatogram (left) of m/z 806.7 ($[M_H + NH_4]^+$) showing the separation of three regioisomers of methylated BMP (18:1)₂ and methylated PG (18:1)₂ along with the respective MS/MS spectra.

spectra of the three regioisomers displayed three characteristic fragment ions patterns. The relative peak intensities of $[M_H + H - H_2O]^+$ and $[MG]_f^+$ are reversed in regioisomers (1)–(3) due to the steric effect. Therefore, the structures of these three regioisomers can be predicted with each acyl chain at the sn-2 position of the glycerol backbone in (1), one acyl chain at sn-1 and the other at sn-2 of each glycerol in (2), and each acyl

chain at the sn-1 position of both glycerol units in (3). However, the PGs exhibited much longer retention times than those of the BMPs due to the enhanced interaction with the stationary phase since the two acyl chains are closely packed in one side of glycerol moiety. These molecules underwent the same cleavage between the phosphate and glycerol unit having the two acyl chains, resulting in the formation of the diacylglycerol fragment ion, $[DG]_f^+$, at m/z 603.8. The latter feature is an indicator that can be used to clearly differentiate the PG structure from BMP, highlighting the capability of nUHPLC-ESI-MS/MS for resolving methylated PGs and BMPs.

The methylation efficiency of TMSD was calculated to be as high as 97% for seven PGPL species, as listed in Table S3. The methylation efficiency was calculated by measuring the original species' peak area before methylation and subtracting that of the unreacted species after methylation in nUHPLC-ESI-MS/MS analysis. However, some species were overmethylated, where the expectations were one methylation for the BMP series and two methylations for the CL series. Overmethylation occurs via additional methylation at the free hydroxide of the PGPL species in low yields. Figure 4 shows the EIC's of CL, MLCL, and DLCL comparing the elution of the following ions: protonated form ($[M_H + H]^+$), ammonium adduct of the methylated form ($[M_H + NH_4]^+$), and ammonium adduct of a single overmethylated (1OM) species $[M_H + 1OM + NH_4]^+$. For CL (18:1)₄ in Figure 4a, the methylated CL species were detected with 1.1% as the protonated form and 95.1% as the ammonium adduct form while 3.7% was detected as the 1OM species. The protonated form was not completely removed with the trial of other ionization modifiers including 5 mM ammonium acetate or a mixture of 5 mM AF and 0.05% ammonium hydroxide. The percentage values were based on the relative peak area ratio of each adduct form without investigating the ionization response factor of each adduct form. Similar observations of the 1OM were found with 4.6% and 7.6% for MLCL (18:2)₃ and DLCL (18:2)₂, respectively. The OM degrees of BMP, BDP, Hemi BDP, and PG species are listed by their relative peak areas in Table 2. It is clear that the amount of 1OM species was 5.6%, 6.9%, 3.1%, and 0%

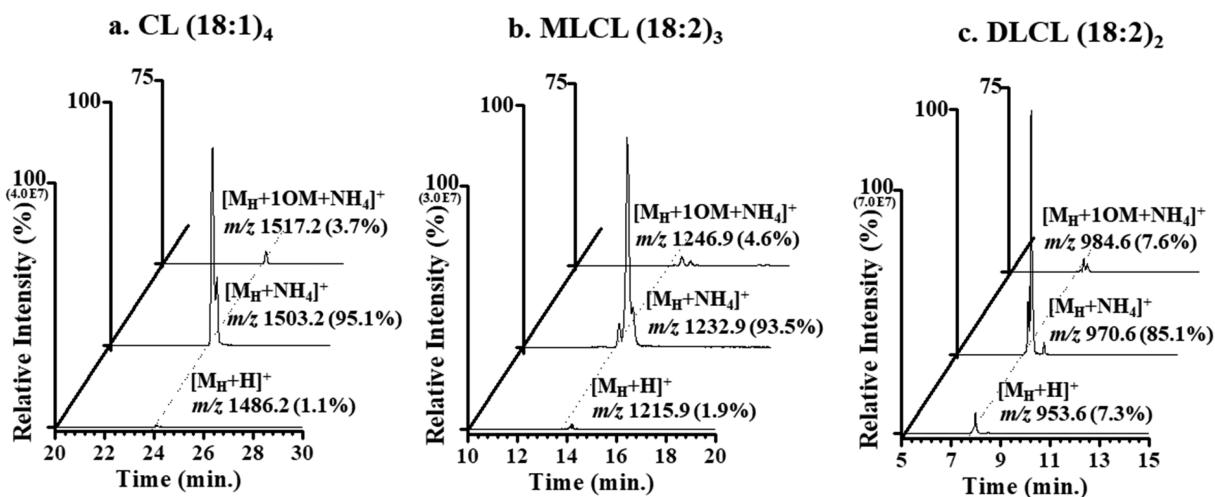


Figure 4. EICs of (1OM) CL species (a) CL (18:2)₄, (b) MLCL (18:2)₃, and (c) DLCL (18:2)₂ as an ammonium adduct ($[M_H + 1OM + NH_4]^+$) compared with the doubly methylated species in ($[M_H + NH_4]^+$) and ($[M_H + H]^+$) forms. The percentage value was based on relative peak area of each form.

Table 2. Relative Peak Areas of Protonated and Ammonium Adduct Forms of the Methylated Species and IOM Form of PG-Based Structural Isomers Obtained by nUHPLC-ESI-MS/MS

detected form	BMP (18:1) ₂		PG (18:1) ₂		Hemi BDP (18:1) ₃		BDP (18:1) ₄	
	<i>m/z</i>	%	<i>m/z</i>	%	<i>m/z</i>	%	<i>m/z</i>	%
[M _H + H] ⁺	789.7	6.8	789.7	3.5	1053.9	N.D.	1318.2	N.D.
[M _H + NH ₄] ⁺	806.7	87.6	806.7	89.6	1070.9	96.9	1335.2	~100
[M _H + IOM + NH ₄] ⁺	820.7	5.6	820.7	6.9	1084.9	3.1	1349.2	N.D.

Table 3. Experimental Peak Area Ratio of the D-/H-Methylated PGPL Standard Mixtures Obtained by SRM Quantification Using nUHPLC-ESI-MS/MS by Varying the Mixing Ratio of D- and H-Methylated Species

PGPL species	observed ratio (D/H)				
	0.25 (2:8) ^a	0.67 (4:6) ^a	1.00 (5:5) ^a	1.50 (6:4) ^a	4.00 (8:2) ^a
PG (14:0) ₂	0.27 ± 0.01	0.71 ± 0.03	1.02 ± 0.03	1.53 ± 0.10	3.77 ± 0.14
PG (18:1) ₂	0.27 ± 0.04	0.71 ± 0.03	1.02 ± 0.07	1.57 ± 0.04	3.80 ± 0.20
BMP (14:0) ₂	0.24 ± 0.00	0.62 ± 0.04	0.93 ± 0.01	1.40 ± 0.12	3.73 ± 0.23
BMP (18:1) ₂	0.26 ± 0.01	0.66 ± 0.02	0.95 ± 0.03	1.40 ± 0.06	3.75 ± 0.31
Hemi BDP (14:0) ₃	0.27 ± 0.02	0.70 ± 0.00	1.00 ± 0.02	1.43 ± 0.02	3.80 ± 0.15
Hemi BDP (18:1) ₃	0.27 ± 0.01	0.69 ± 0.01	0.96 ± 0.04	1.42 ± 0.05	3.72 ± 0.14
BDP (18:1) ₄	0.27 ± 0.01	0.71 ± 0.05	1.07 ± 0.08	1.50 ± 0.02	3.78 ± 0.26
DLCL (18:2) ₂	0.27 ± 0.00	0.71 ± 0.03	1.04 ± 0.07	1.44 ± 0.06	3.74 ± 0.30
MLCL (18:2) ₃	0.26 ± 0.01	0.69 ± 0.01	0.98 ± 0.03	1.41 ± 0.03	3.77 ± 0.28
CL (14:0) ₄	0.27 ± 0.01	0.69 ± 0.02	1.07 ± 0.02	1.48 ± 0.02	3.81 ± 0.21

^aMixing ratio of each methylated PGPL.

(n.d.) for BMP (18:1)₂, PG (18:1)₂, Hemi BDP (18:1)₃, and BDP (18:1)₄, respectively.

To quantify the methylated PGPLs without the complication of correcting for the overmethylated species, a relative quantification based on ILM²⁷ was applied by analyzing the pairs of H- and D-methylated PGPL species. A total of 10 H- and D-methylated PGPL standards were mixed in five D/H ratios of 0.25 (2:8), 0.67 (4:6), 1.00 (5:5), 1.50 (6:4), and 4.00 (8:2). The experimental D/H ratio of each species was calculated from the peak area measurements of each pair obtained via nUHPLC-ESI-MS/MS, which are listed in Table 3. Quantification was based on SRM utilizing different CID energies specific for each lipid class, and the precursor/quantifier ions are listed in Table S1. Deviation of the observed D/H from the mixing ratio was 4.1–6.8%, which is reasonable for use within the 16-fold range of changes observed.

ILM-Based Relative Quantification of PGPLs from Parkinson's Model Human Dopaminergic Cells. ILM-based relative quantification of PGPLs was applied to human dopaminergic SH-SY5Y cells treated with three commonly used drugs (6-OHDA, MPP⁺, and rotenone) to induce Parkinson's disease. Cell viabilities were approximately 50% for all treatments when measured at 24 h after the drug treatments, as shown in Figure S3. Prior to quantification, each lipid extract of the drug treated SH-SY5Y cells were H-methylated and analyzed by nUHPLC-ESI-MS/MS (see the BPCs in Figure S4) to identify the PGPLs. Structural determination using data-dependent CID experiments of the lipid extracts of the control and drug treated cells yielded a total of 229 unique PGPLs including 11 PG, 9 BMP, 16 Hemi BDP, 1 BDP, 71 MLCL, and 121 CL species, without counting regioisomers.

Although all identified lipid species were not completely separated, they can be identified from MS/MS spectra obtained by data-dependent CID experiments. Figure S5a shows the extracted ion chromatograms of CL species having acyl chains of total carbon number as 66, 68, and 70 from the

top but different numbers of double bonds, representing that CL species with a higher degree of unsaturation eluted earlier than saturated CL species. While the three CL species (66:3, 68:4, 70:5) eluted at the same retention time (*t_r* = 24.4 min) were detected in the precursor MS scan in Figure S5b, data-dependent MS/MS experiments provided CID spectra of each species (Figure S5c) in sequence, resulting in the determination of molecular structures from the characteristic fragment ions of each CL species. The molecular structures, including acyl chain types, of the 229 PGPLs are listed in Table S4. The number of identified PGPL species, especially MLCLs and CLs, is much larger than those reported previously²⁷ and is the highest number reported to date to the best of our knowledge. For ILM-based quantification, each lipid extract of the drug treated cells was D-methylated and that of the control cells was H-methylated. A mixture of equal aliquots of D- and H-methylated pairs was analyzed in SRM mode using nUHPLC-ESI-MS/MS. For SRM quantification, the quantifier ions, mostly [MG_i]⁺ or [DG_i]⁺ as listed in Table S1, were selected from MS/MS spectra after confirmation of the precursor ion for each PGPL class. The molecular structure and calculated D/H ratio of each PGPL species upon drug treatment are listed in Table S4. The overall change in PGPL species was visualized using a heat map plotted with the D/H ratios of 105 PGPL species showing >2-fold changes (Figure S6). The species were categorized as follows: PGPLs with (a) saturated or monounsaturated fatty acyl chains and (b) polyunsaturated fatty acyl (PUFA) chains. The drug treatments of the human dopaminergic cells resulted in significant changes in most PGPL levels. In particular, most concentrations of MLCL species, regardless of the unsaturation degree of the acyl chains, were significantly reduced, with a few exceptions showing increases (Figure S6b). These compounds were not quantifiable in the control sample but were detected in the drug treated samples. Moreover, the levels of monounsaturated CL species decreased to a certain degree, while those of polyunsaturated CLs increased. The fold changes (D/H) of

PG, BMP, BDP, and Hemi BDP species were plotted in Figure 5a and showed that three PGs (34:1, 34:2, and 36:2) and BMP 18:1_18:1 were significantly stimulated by the drugs.

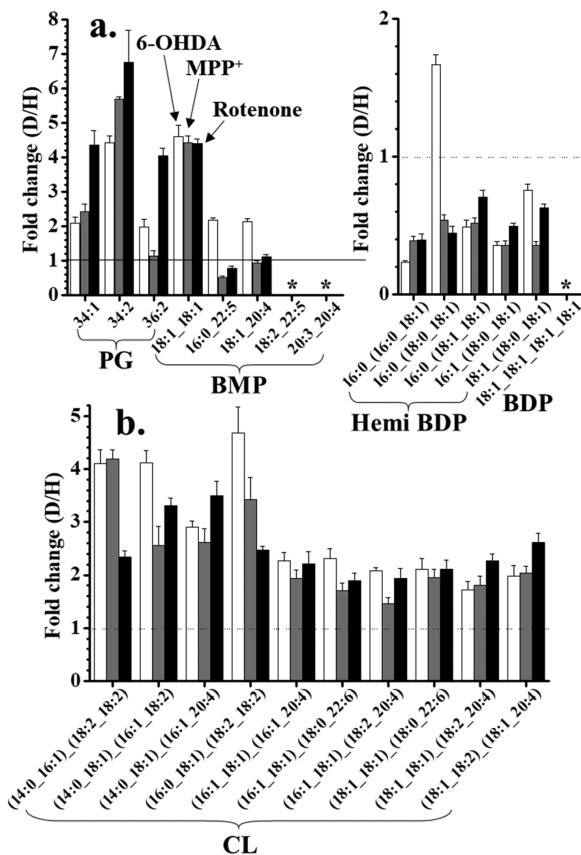


Figure 5. Fold change (D/H) of (a) PG, BMP, Hemi BDP, and BDP and (b) CLs showing >2-fold changes upon drug treatment. Species with * were quantified from the control cell extract but were not quantifiable after drug treatment.

In contrast, some structural isomers of BMP (18:2_22:5 and 20:3_20:4) were not quantifiable in the drug treated samples. In addition, the levels of 5 Hemi BDP species were mostly decreased (>2-fold) except for that of Hemi BDP 16:0_(18:0_18:1) in the 6-OHDA treatment. BMP can be produced from the deacylation of PG by phospholipase A₂ (PLA₂) to produce LPG and sequentially acylated via acyl transferase.^{3,13} It can also be formed via acylation of PG to produce Hemi BDP followed by deacylation to BMP via PLA₂.¹³ Thus, it is likely that the levels of BMP and Hemi BDP were reduced due to drug-induced perturbation, which simultaneously increased PG levels. In this study, BDP 18:1_18:1_18:1_18:1 was quantified in the control sample but was not quantifiable in the drug treated samples. No BDP has been detected from the cellular extracts to date. Figure 5b shows the D/H ratios of 10 significantly increased CL species, 7 of which contain arachidonic (AA or 20:4) or docosahexanoic (DHA or 22:6) fatty acyl chains, as compared to most CLs whose levels decreased (Figure S6). This can be attributed to the pathological remodeling of CLs to enrich DHA and other PUFAs in CL which have been reported to cause mitochondrial dysfunction and increase the oxidant production.¹⁰

CONCLUSIONS

Methylation significantly enhanced the separation and detection of PGPLs, as demonstrated by the increased S/N ratio. ILM-based analysis improved the characterization and quantification of PGPLs including Hemi BDP, BDP, DLCL, and MLCL species, which have rarely been reported in the literature due to their relatively low abundance and poor intact molecule detection via MS. Furthermore, this study demonstrated the complete separation of the regioisomers of each PGPL species by nUHPLC separation supported by differences in geometrical structures determined from their respective MS/MS spectra. In addition, BMPs and PGs with the same acyl chains, structural isomers, were clearly distinguished by baseline separation and CID spectra, highlighting the utility of PGPL methylation. The methylation efficiency of the PGPLs was >97%, although some over-methylation products were observed. However, the ILM-based SRM quantification using nUHPLC-ESI-MS/MS provided target-specific analysis of methylated products and quantifier ions with <6.8% relative deviation for determination of the experimental ratio of D- and H-methylated products over a 16-fold mixing ratio range. When the ILM method was applied to control SH-SY5Y dopaminergic cells and those treated with drugs to induce Parkinson's disease, a total of 229 unique PGPLs, including 16 Hemi BDP, 71 MLCL, and 121 CL species, were identified and relatively quantified. Although CL and MLCL were analyzed by LC-MS^{19,20} and MALDI-TOF/MS³⁷ in the literature, the identified number of CL species were limited (28 CL and 2 MLCL) due to the poor ionization of intact CL species in the MS analysis. The present study represents the highest number of PGPLs reported to date. Since the PGPL levels were significantly influenced by drug treatments, the ILM method can be used for the study of oxidative stress on CLs and their associated remodeling, which is closely related to mitochondrial membrane rigidity. This method also shows promise for the identification of potential biomarkers to diagnose disease. This study expanded the capability of ILM-based relative quantification of lipids using nUHPLC-ESI-MS/MS for low abundance PGPLs, showing significant PGPL detection sensitivity enhancement.

ASSOCIATED CONTENT

Supporting Information

The Supporting Information is available free of charge on the ACS Publications website at DOI: 10.1021/acs.analchem.9b00800.

Regioisomer structures of PGPL species; proposed CID mechanism of the two regioisomers of MLCL; cell viability after treatment with the three different compounds; base peak chromatograms of the methylated lipid extracts; extracted ion chromatograms, MS spectra, and data-dependent CID (MS/MS) spectra; heat maps; types of precursor/quantifier ion for SRM quantification by nUHPLC-ESI-MS/MS and the collision energy assigned for each PGPL class by ILM; LOD and LOQ values of intact and methylated PGPL standards; methylation efficiency of PGPLs with TMSD; fold change (D/H) of D-methylated (drug treated) to H-methylated (control) PGPLs by nUHPLC-ESI-MS/MS (PDF)

■ AUTHOR INFORMATION

Corresponding Author

*Phone: (82) 2 2123 5634. Fax: (82) 2 364 7050. E-mail: mhmoon@yonsei.ac.kr.

ORCID 

Myeong Hee Moon: 0000-0002-5454-2601

Notes

The authors declare no competing financial interest.

■ ACKNOWLEDGMENTS

This study was supported by a grant (NRF-2018R1A2A1A05019794) from the National Research Foundation of Korea.

■ REFERENCES

- (1) Hostetler, K. Y. Polyglycerophospholipids: phosphatidylglycerol, diphosphatidylglycerol and bis (monoacylglycerol) phosphate. In *New Comprehensive Biochemistry*; Elsevier B.V.: London, 1982; Chapter 6, pp 215–261.
- (2) Kobayashi, T.; Stang, E.; Fang, K. S.; de Moerloose, P.; Parton, R. G.; Gruenberg, J. *Nature* **1998**, *392* (6672), 193–197.
- (3) Hullin-Matsuda, F.; Kawasaki, K.; Delton-Vandenbroucke, I.; Xu, Y.; Nishijima, M.; Lagarde, M.; Schlame, M.; Kobayashi, T. *J. Lipid Res.* **2007**, *48* (9), 1997–2008.
- (4) Hullin-Matsuda, F.; Luquain-Costaz, C.; Bouvier, J.; Delton-Vandenbroucke, I. *Prostaglandins, Leukotrienes Essent. Fatty Acids* **2009**, *81* (5–6), 313–24.
- (5) Liu, N.; Tengstrand, E. A.; Chourb, L.; Hsieh, F. Y. *Toxicol. Appl. Pharmacol.* **2014**, *279* (3), 467–76.
- (6) Hein, L. K.; Duplock, S.; Fuller, M. *J. Lipid Res.* **2013**, *54* (6), 1691–1697.
- (7) Ren, M.; Phoon, C. K.; Schlame, M. *Prog. Lipid Res.* **2014**, *55*, 1–16.
- (8) Paradies, G.; Paradies, V.; De Benedictis, V.; Ruggiero, F. M.; Petrosillo, G. *Biochim. Biophys. Acta, Bioenerg.* **2014**, *1837* (4), 408–17.
- (9) Paradies, G.; Paradies, V.; Ruggiero, F. M.; Petrosillo, G. *Antioxid. Redox Signaling* **2014**, *20* (12), 1925–53.
- (10) Shi, Y. *J. Biomed. Res.* **2010**, *24* (1), 6–15.
- (11) Ikon, N.; Ryan, R. O. *Lipids* **2017**, *52* (2), 99–108.
- (12) Fobker, M.; Voss, R.; Reinecke, H.; Crone, C.; Assmann, G.; Walter, M. *FEBS Lett.* **2001**, *500* (3), 157–162.
- (13) Record, M.; Amara, S.; Subra, C.; Jiang, G.; Prestwich, G. D.; Ferrato, F.; Carriere, F. *Biochim. Biophys. Acta, Mol. Cell Biol. Lipids* **2011**, *1811* (7–8), 419–30.
- (14) Scherer, M.; Schmitz, G. *Chem. Phys. Lipids* **2011**, *164* (6), 556–62.
- (15) Chicco, A. J.; Sparagna, G. C. *Am. J. Physiol Cell Physiol.* **2007**, *292* (1), C33–44.
- (16) Claypool, S. M.; Koehler, C. M. *Trends Biochem. Sci.* **2012**, *37* (1), 32–41.
- (17) Tyurin, V. A.; Tyurina, Y. Y.; Osipov, A. N.; Belikova, N. A.; Basova, L. V.; Kapralov, A. A.; Bayir, H.; Kagan, V. E. *Cell Death Differ.* **2007**, *14* (4), 872–5.
- (18) van Werkhoven, M. A.; Thorburn, D. R.; Gedeon, A. K.; Pitt, J. *J. Lipid Res.* **2006**, *47* (10), 2346–51.
- (19) Minkler, P. E.; Hoppel, C. L. *J. Lipid Res.* **2010**, *51* (4), 856–65.
- (20) Bird, S. S.; Marur, V. R.; Sniatynski, M. J.; Greenberg, H. K.; Kristal, B. S. *Anal. Chem.* **2011**, *83* (3), 940–9.
- (21) Scherer, M.; Schmitz, G.; Liebisch, G. *Anal. Chem.* **2010**, *82* (21), 8794–9.
- (22) Vosse, C.; Wienken, C.; Cadenas, C.; Hayen, H. *J. Chromatogr A* **2018**, *1565*, 105–113.
- (23) Wang, M.; Palavicini, J. P.; Cseresznye, A.; Han, X. *Anal. Chem.* **2017**, *89* (16), 8490–8495.
- (24) Lee, J. W.; Nishiumi, S.; Yoshida, M.; Fukusaki, E.; Bamba, T. *Journal of Chromatography A* **2013**, *1279*, 98–107.
- (25) Kim, S. H.; Song, H. E.; Kim, S. J.; Woo, D. C.; Chang, S.; Choi, W. G.; Kim, M. J.; Back, S. H.; Yoo, H. J. *J. Lipid Res.* **2017**, *58* (2), 469–478.
- (26) Cai, T. X.; Shu, Q. B.; Hou, J. J.; Liu, P. B.; Niu, L. L.; Guo, X. J.; Liu, C. C.; Yang, F. Q. *Anal. Chem.* **2015**, *87* (1), 513–521.
- (27) Lee, J. C.; Byeon, S. K.; Moon, M. H. *Anal. Chem.* **2017**, *89* (9), 4969–4977.
- (28) Bose, A.; Beal, M. F. *J. Neurochem.* **2016**, *139* (Suppl 1), 216–231.
- (29) Perrett, R. M.; Alexopoulou, Z.; Tofaris, G. K. *Mol. Cell. Neurosci.* **2015**, *66* (Pt A), 21–28.
- (30) Wang, X.; Wang, W.; Li, L.; Perry, G.; Lee, H. G.; Zhu, X. *Biochim. Biophys. Acta, Mol. Basis Dis.* **2014**, *1842* (8), 1240–7.
- (31) Xicoy, H.; Wieringa, B.; Martens, G. J. *Mol. Neurodegener.* **2017**, *12* (1), 10.
- (32) Giordano, S.; Lee, J.; Darley-Usmar, V. M.; Zhang, J. H. *PLoS One* **2012**, *7* (9), e44610.
- (33) Byeon, S. K.; Lee, J. Y.; Moon, M. H. *Analyst* **2012**, *137* (2), 451–8.
- (34) Lee, J. Y.; Yang, J. S.; Park, S. M.; Byeon, S. K.; Moon, M. H. *J. Chromatogr A* **2016**, *1464*, 12–20.
- (35) Lim, S.; Byeon, S. K.; Lee, J. Y.; Moon, M. H. *J. Mass Spectrom.* **2012**, *47* (8), 1004–1014.
- (36) Byeon, S. K.; Kim, J. Y.; Lee, J. S.; Moon, M. H. *Anal. Bioanal. Chem.* **2016**, *408* (9), 2265–74.
- (37) Lopalco, P.; Stahl, J.; Annese, C.; Averhoff, B.; Corcelli, A. *Sci. Rep.* **2017**, *7* (1), 2972.